Scaling of divertor heat flux profile widths in DIII-D

C.J. Lasnier[1], M.A. Makowski[1], J.A. Boedo[2], N.H. Brooks[3], D.N. Hill[1], A.W. Leonard[3], and J.G. Watkins[4]

e-mail:Lasnier@LLNL.gov

[1]Lawrence Livermore National Laboratory, Livermore, California, USA
[2]University of California-San Diego, La Jolla, California 92093-0417, USA
[3]General Atomics, PO Box 85608, San Diego, California 92186-5608, USA
[4]Sandia National Laboratories, Albuquerque, New Mexico, USA

Abstract. Recent experiments in DIII-D have led to a new empirical scaling of divertor heat flux width $\lambda_{q,div}$ as a function of plasma parameters. Previous scaling efforts around the world have produced results that are not in agreement with each other. We controlled conditions during parameters scans as closely as possible to prevent other complicating variations. We varied B_T at constant I_p, I_p at constant B_T, and B_T/I_p at constant q_{95}. The neutral beam injected power was changed at constant I_p and B_T. Line-averaged density was varied at constant I_p and B_T. We find $\lambda_{q,div}$ is principally dependent on the plasma current to the -1.24 power. Our results agree with previous conduction-limited scalings from JET and NSTX, and exclude other scalings from both JET and other devices.

1. Introduction

The width of the divertor heat flux profile $\lambda_{q,div}$ is of great interest in future large tokamaks as well as many present devices. Previous studies examining the parametric dependence of $\lambda_{q,div}$ have arrived at diverse scalings [1] in JET [2], ASDEX-Upgrade [3], JT60-U [4,5], DIII-D [6,7], and NSTX [8]. With the aim of resolving this disagreement, we performed measurements in lower single-null edge localized mode (ELM)ing H-mode diverted configurations. We varied toroidal field (B_T) at constant plasma (I_p), I_p at constant B_T, and B_T/I_p at constant q_{95}. The neutral beam injected power P_{inj} was changed at constant I_p and B_T. Line-averaged density $\bar{n}_e$ was varied at constant I_p and B_T. The divertor heat flux was calculated from infrared camera measurements using a new high-resolution fast-framing IR camera.

The IR camera recorded divertor plate surface thermal emission at multi-kilohertz frame rates through the whole discharge, so that time-averaged data as well as rapid changes due to ELMs were obtained. The heat flux at each position in the radial profile was calculated at each of the times steps using the THEODOR 2D heat flux analysis code [9]. The THEODOR code has a capability of including a surface layer of arbitrary effective thickness to account for fast surface cooling often observed during transients. This layer must be chosen empirically using the surface temperature history. In order to make the simplest possible assumptions, no surface layer effects were assumed in the heat flux calculation. This results in some overshoot when the surface temperature falls after an ELM pulse. Consequently, we avoid the time slices immediately after an ELM in this analysis.

In an effort to separate the physics of ELM heat flux scaling from the scaling of the inter-ELM heat flux, we chose time slices least affected by ELMs. Therefore heat flux data was averaged from a time 20% into the inter-ELM interval until 95% of the way to the onset of

the subsequent ELM, prior to exponential profile fitting. This fixed fraction of the ELM period was chosen so as to reduce the impact of overshoot in the heat flux calculation resulting from the previous ELM, due to the effect of surface layers mentioned above. The overshoot is most pronounced immediately after the ELM heat flux peak and then falls off with time.

The heat flux profiles were coherently averaged for these inter-ELM times over multiple inter-ELM intervals of nearly fixed conditions.

The outer strike point heat flux profile was mapped to outer midplane and fitted on the public and private flux side with separate exponential ($a_0 + a_1 e^{x/\lambda}$) profiles (Fig. 1) [10]. The heat flux width $\lambda_{q,div,midplane}$ is taken to be the sum of the two exponential widths. This is different from the integral width proposed by Loarte [11], in which the integral of the profile is divided by the peak. Our heat flux profiles show plateau values in the private flux and far scrape-off-layer (SOL), at a level too large to be accounted for by absorbed radiation or plasma interaction. It is possible that there is some effect of internal optical reflections. The plateau effect is still being investigated. Due to these flat areas in the common and the private flux areas far from the separatrix, the Loarte width would depend on the arbitrary width of the integration window, and so is unsatisfactory measure here whereas the sum of the exponential widths is not sensitive to this parameter.

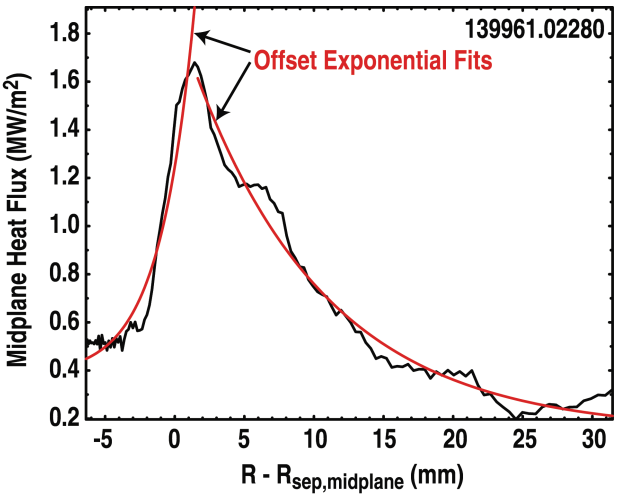

FIG. 1. Typical heat flux profile after mapping to the midplane as a function of distance from the separatrix at the midplane, R-$R_{sep,mp}$, showing offset exponential fits.

Heat flux data was averaged from a time 20% into the inter-ELM interval until 95% of the way to the onset of the subsequent ELM, prior to exponential fitting. This fixed fraction of the ELM period was chosen so as to reduce the impact of overshoot in the heat flux calculation resulting from the previous ELM, due to the effect of surface layers mentioned above. The overshoot is most pronounced immediately after the ELM heat flux peak and then falls off with time.

We show scaling of the profile width as a function of the parameters varied, and compare with published results from other devices.

2. Variation in $\lambda_{q,div}$ with Plasma Parameters

Multi-parameter fits were made to investigate the scaling of $\lambda_{q,div}$ with I_p (plasma current), q_{95} (safety factor at the 95% flux surface), n_e (electron density), B_T (toroidal field), P_{SOL} [power flow into the SOL], P_{inj} (neutral beam injected power), s_{95} (magnetic shear at the 95% flux surface), and α_{95} (dimensionless pressure gradient at the 95% flux surface).

In Fig. 2, for the case with averaging over ELMs [12], the full widths at half maximum (FWHM) of the heat flux in the divertor are shown plotted against line-averaged density. The FWHM is used here because the heat flux profiles at higher density are not well-fit by the exponentials defined above. At low density, $\lambda_{q,div}$ is independent of $\bar{n}_e$, but there is a threshold density of ~7x10^{19} m^{-3} where the profile becomes wider, representing the onset of detachment. In the density scan from which this data was extracted, P_{in} was 4.9–5.1 MW, except for the densities $\bar{n}_e = 5.2\times10^{19}$ m^{-3} and $\bar{n}_e = 6.8\times10^{19}$ m^{-3} where P_{in} = 7.2 MW, and P_{in} = 4.1 MW, respectively. Since we found $\lambda_{q,div}$ does not depend on input power, this power variation does not affect the widths obtained from the density scan at these densities. Toroidal field was held constant at B_T = -1.9 T, and plasma current was held at I_p = 1.3 MA.

The effect of radiation from the outboard divertor on the strike point heat flux profile is small for the low-density attached discharges. It becomes significant at the onset of detachment where we see the profile broadening, and in fully detached strike points not considered here, the radiated power absorbed by the divertor plate accounts for nearly all the measured heat flux.

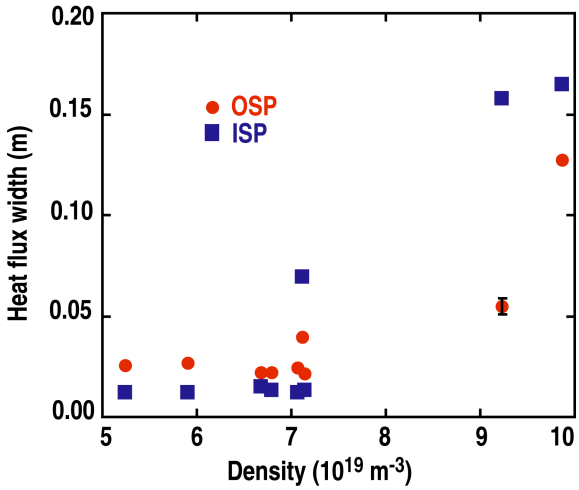

FIG. 2. Dependence of divertor heat flux profile width on density. There is essentially no effect below the detachment threshold. A representative error bar is shown on the red point at lower right.

We find that $\lambda_{q,div,midplane}$ is larger at low plasma current, as shown in Fig. 3 [10], where $\lambda_{q,div,midplane}$ is plotted against I_p. The width decreases inversely as a power of the plasma current close to unity, namely $\lambda_{q,div,midplane}$ (mm) = $6.38/I_p^{1.24}$ (MA). Similar behavior is seen in NSTX [8] where the width decreases with increasing plasma current, approximately as $1/I_p$.

The error bar for $\lambda_{q,div,midplane}$ is ±0.5 mm. A representative error bar is shown for a data point in Fig. 3, but is otherwise omitted in this and succeeding figures so as not to obscure the data points.

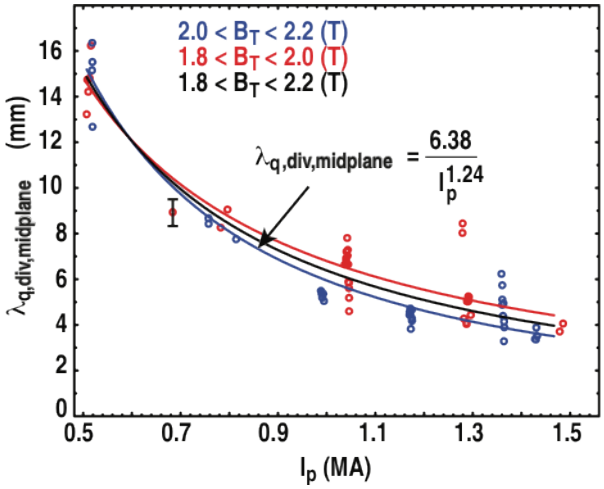

FIG. 3. Dependence of heat flux width (mapped to the midplane) on plasma current. The red and blue symbols denote two ranges of toroidal field, showing little effect from changing B_T. A representative error bar is shown.

We know that core plasma confinement improves at higher plasma current [13], and the behaviour observed is consistent with cross-field SOL transport also being reduced as plasma current increases. For this scan of plasma current, toroidal field was held fixed

at B_T = -1.9 T, and P_{inj} = 4.7–5.0 MW, except for the point at I_p = 1.3 MA where P_{inj} = 4.1 MW. Density was not held constant, but allowed to vary at the natural H-mode density, because of practical difficulty measuring the heat flux at the OSP during the plasma pumping that would have been required to maintain constant density. Figure 4 [12] shows the line-averaged density variation during the I_p scan. Note that the range of densities is within the zone of Fig. 2 where the density variation shows little effect on the heat flux width. Also, the density remains at low Greenwald fraction as I_p is raised and consequently the detachment threshold is raised along with the density. Therefore the density variation during the I_p scan does not affect the heat flux width.

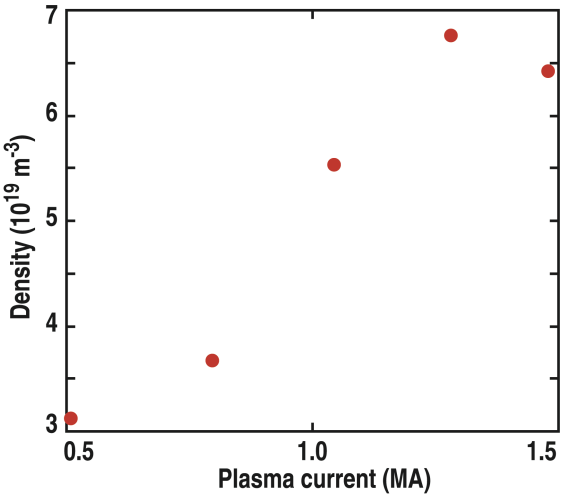

FIG. 4. Variation of line-averaged electron density during the plasma current scan. All these densities are at the low end of Fig. 3, so there was little effect of the density variations on the heat flux width.

For the inter-ELM data, the widths $\lambda_{q,div,midplane}$ showed no discernable trend in the multi-parameter fits with toroidal field B_T, in contrast to the case where the data was averaged over ELMs [12]. We varied B_T from 1.2 to 2.1 T (ion ∇B drift toward the lower divertor). No correlation was seen between $\lambda_{q,div}$ and B_T. The dependence on plasma current but not toroidal field is not fully understood.

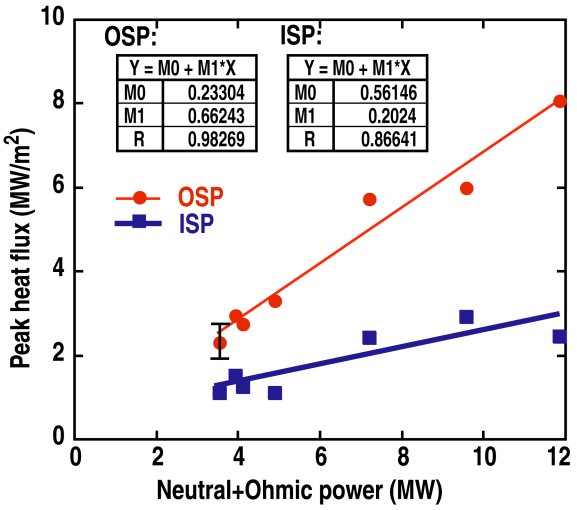

FIG. 5. *ELM-averaged peak heat flux at the ISP and OSP plotted against the input power. Linear fits to the data are plotted, with fitting parameters shown in the boxes. The dependence on input power appears linear. A representative error bar is shown.*

We found both in the present analysis between ELMs and the previous analysis averaged over ELMs [12] only very weak dependence of $\lambda_{q,div}$ on total input power P_{in}, which in these discharges is the sum of P_{inj} and the Ohmic heating power.

We illustrate this in Fig. 5, where peak heat flux averaged over ELMs is plotted against input power. The peak heat flux increases linearly with input power. By conservation of energy, the heat flux profile width stays fixed. As found on NSTX, JET and ASDEX-Upgrade (DIVII), we find essentially no (or very weak) dependence of the width on input power.

3. Divertor Heat Flux Profile Width in Relation to Upstream Temperature

Figure 6 [10] shows typical T_e (electron temperature) and n_e (electron density) profiles at the outer midplane derived from Thomson scattering measurements in the upper outer SOL. Typically 10–20 profiles were coherently averaged over a 200 ms window, from time slices just before ELMs. The Thomson profile data were mapped along field lines to the outer midplane. For each parameter (n_e and T_e) exponential fits were made to the data near the separatrix, from inside and outside, which gave the electron temperature gradient scale lengths, λ_{Te}^{int} and λ_{Te}^{SOL}, respectively. The λ_{Te}^{SOL} was found to have less scatter than either the λ_{Te}^{int} or a hyperbolic tangent fit width. The fitted λ_{Te}^{SOL} is not sensitive to the method of determining the separatrix location. The divertor heat flux profile widths $\lambda_{q,div,midplane}$ were compared with upstream λ_{Te}^{SOL}, showing a very weak correlation (Fig. 7) [10]. This is contrary to two-point models that give that predict $\lambda_{Te} = (7/2)\,\lambda_q$ [14].

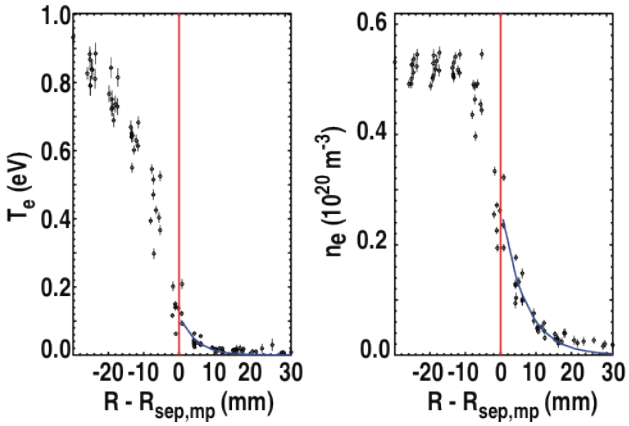

FIG. 6. Typical outer midplane electron temperature and density profiles mapped from Thomson scattering measurements to the outer midplane. The curves show the exponential fits.

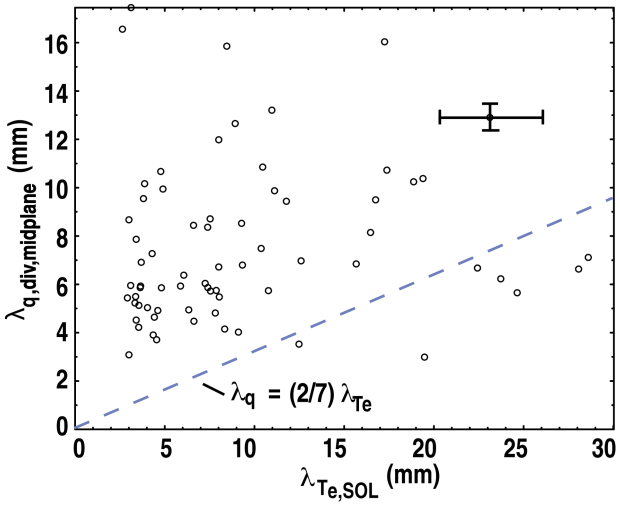

FIG. 7. Plot of the heat flux width, $\lambda_{q,div,midplane}$, versus the Thomson electron temperature profile e-folding length in the scrape off layer, λ_{Te}^{SOL}. The widths are larger than expected from a two point model, λ_q = (2/7) λ_{Te}, which is shown by the blue dashed line.

We can conclude that the heat flux profiles for the most part are wider than predicted by the two-point model. Departures from that model are to be expected due to the presence of radial transport, radiation within the transport volume, and neutral transport in the divertor, which these two-point models neglect.

4. Comparison with Other Scaling Results

The results of the present scaling study are in rough agreement with the JET scaling of conduction limited heat flux widths [15], given by

$$\lambda_{q,div,midplane}^{JET}\,(\mathrm{mm}) = 2.41\times10^{-5}\,B_T^{-1}(\mathrm{T})\,P_{SOL}^{-1/2}\,(\mathrm{MW})\,n_e^{1/4}\left(\mathrm{m}^{-3}\right)q_{95}R^2\,(\mathrm{m}) \quad . \qquad (1)$$

The comparison between the present DIII-D scaling and Eq. (1) is shown in Fig. 8 [10]. The dominant dependence is in $q_{95}/B_T \sim 1/I_p$. The density dependence is weak in the JET scaling

law, in agreement with our observations. However, our fits show no dependence on P_{SOL}, the power crossing the separatrix. With no machine size variation in our data to compare with the R^2 dependence from JET, we are left with $1/I_p$ from Eq. (1), which is similar to our finding. Our finding of no dependence of the width on input power is in direct contrast to Eq. (1).

The heat flux width prediction from Ref. [5] was also considered:

$$\lambda^{\text{H-2}}_{\text{q,div,midplane}}\ (\text{mm}) = 5.3 P^{0.38}\ (\text{MW})\ B_T^{-0.71}(\text{T})\ q_{95}^{0.3} \quad . \tag{2}$$

The widths predicted by Eq. (2) are 10 times smaller than those found in DIII-D [10]. Equation (2) contains no scaling for machine size.

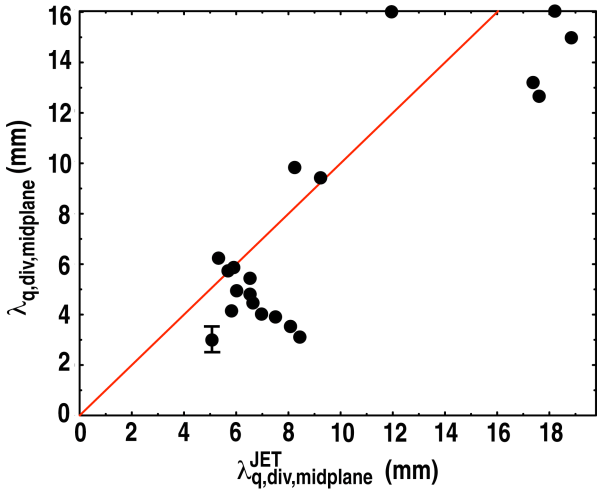

FIG. 8. Comparison of DIII-D heat flux profile width with the JET conduction-limited scaling applied to the same DIII-D data. The red line has a slope of unity. The DIII-D results are in reasonable agreement with the JET scaling. A representative error bar is shown.

5. Comparison of Divertor Heat Flux Profiles with UEDGE Modeling

Modeling of discharges from the plasma current scan using the UEDGE code [16] has been initiated, in an attempt to identify what physical mechanism causes the heat flux width to change with plasma current. The power flow through the SOL, and the midplane electron temperature and density profiles are taken from the experimental data. However, there is sufficient scatter in the experimental electron temperature and density data that widely varying profiles could be chosen that are all within the error bars. Transport coefficients in UEDGE are adjusted until the upstream profiles agree with the experiment. In the results reported here, best agreement with the heat flux width was obtained when drifts were turned on at 20% of full value, and poor agreement when drifts were turned off. The comparison between the experimentally determined heat flux profile and the UEDGE output for I_p = 1.5 MA, the highest plasma current reached in the I_p scan, is shown in Fig. 9 [10] as a function of poloidal distance along the horizontal divertor surface. The experimental data are much lower than the UEDGE prediction, and the data are multiplied by a factor of 5.2 in the plot to match the UEDGE prediction at its peak value. The uncertainty in the upstream

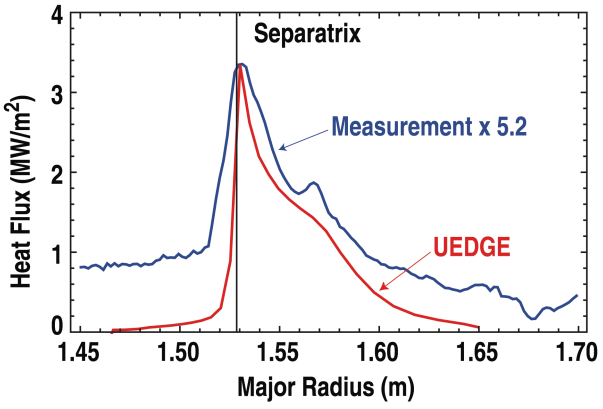

FIG. 9. Comparison of measured heat flux (blue, multiplied by 5.2) and that predicted by UEDGE (blue) [10]. For this case I_p =1.5 MA.

profiles creates a large margin of error in the UEDGE predictions of divertor heat flux and other divertor parameters. In addition, it is possible in the experiment to have heat deposited in unobserved locations whereas UEDGE, to achieve power balance, places that heat at the outer strike point. Further work is needed to reconcile these differences.

The measured radiated power was 350 kW. This value was approximately matched in UEDGE (300 kW) when the flows were turned on at 20%, but the code greatly underestimated the radiated power (90 kW) when drifts were turned off. The heat flux profile in the model was narrower than in the experiment. Some degree of shoulder in seen in both the measured and experimental profile.

These preliminary attempts at UEDGE modeling are the beginning of a more in-depth effort to compare these measurements with modeling and to aid in understanding the physical origin of the scaling with plasma current. It is clear that drifts are important in interpreting the result, but we must obtain agreement with experimental data with drifts fully turned on.

6. Conclusion

In DIII-D, we find the strongest dependence of the divertor heat flux profile width is on the plasma current. The heat flux width varies inversely as the 1.24 power of the plasma current and not at all with input power. Our result is in substantial agreement with the conduction-limited JET scaling of Ref. [15] for plasma current but not for power, but not at all with the multi-machine scaling of Ref. [5]. We are not able to confirm any dependence of the heat flux width on the near-separatrix SOL fall-off length of the outer midplane temperature profile, although we find the simple two-point models do not provide an adequate description of the heat flux transport. Our heat flux profiles are substantially wider than predicted by the two-point model. We find no evidence in the multi-parameter fitting of a significant dependence on B_T or P_{SOL}. The lack of change in heat flux profile width in spite of the change in field line connection length with B_T indicates reduction in cross-field SOL transport with B_T. The physical mechanism leading to the scaling of λ_q with I_p is not yet understood, but we note that increasing I_p is known to reduce radial transport inside the separatrix and we suspect a similar effect in the SOL. Attempts to compare the data with the UEDGE modeling code have begun, and we find that drifts are important in matching the heat flux profile width. At this point we still see substantial differences between the model and experiment. Further modeling will be done to help understand the I_p dependence of the heat flux profile.

This work was supported by the US Department of Energy under DE-AC52-07NA27344, DE-FG002-07ER4917, DE-FC02-04ER54698, and DE-AC04-94AL85000.

References

[1] LOARTE, A., *et al.,* Nucl Fusion **47** (2007) S203
[2] EICH, T., *et al.,* J. Nucl. Mater. **333-339** (2005) 669
[3] HERRMANN, A., Plasma Phys. Control. Fusion **44** (2002) 883
[4] ITER Physics Basis Editors, Nucl. Fusion **39** (1999) 2137

[5] LOARTE, A., *et al.,* J. Nucl. Mater. **266-269** (1999) 587
[6] HILL, D.N., *et al.,* J. Nucl. Mater **196-198** (1992) 204
[7] LASNIER, C.J., *et al.,* Nucl. Fusion **38** (1998) 1225
[8] MAINGI, R., *et al.,* J. Nucl. Mater **363-365** (2007) 196
[9] HERRMANN, A., *et al.*, Plasma Phys. Control. Fusion **37** (1995) 17
[10] MAKOWSKI, M.A., *et al.,* "Comparison of Upstream T_e Profiles with Downstream Heat Flux Profiles and Their Implications on Parallel Heat Transport in the SOL in DIII-D," Proc. of 19th International Conference on Plasma-Surface Interactions, San Diego, CA, 2010 and submitted for publication in J. Nucl. Mater.
[11] LOARTE, A., *et al.*, J. Nucl. Mater. **266-269** (1999) 587
[12] LASNIER, C.J., *et al.*, Proc. of 36th EPS Conference on Plasma Phys., Sofia, 2009 ECA Vol. 33E, P-4.140
[13] CORDOY, J.G. and ITER Confinement Database and Modeling Working Group, Plasma Phys. Control. Fusion **39** (1997) B115–B127
[14] PITCHER, C.S. AND STANGEBY, P.C., Plasma Phys. Control. Fusion **39** (1997) 779
[15] KIRNEV, G., *et al.*, Plasma Phys. Control. Fusion **49** (2007) 689
[16] ROGNLIEN, T., *et al.,* J. Nucl. Mater. **196-198** (1992) 347